DOI 10.1007/s11106-022-00272-2
Powder Metallurgy and Metal Ceramics, Vol. 60, Nos. 9-10, January, 2022 (Russian Original Vol. 60, Nos. 9-10, Sept.-Oct., 2021)

TRIBOLOGICAL PROPERTIES OF $ZrN–Si_3N_4–TiN$ COMPOSITES CONSOLIDATED BY SPARK PLASMA SINTERING

O.B. Zgalat-Lozynskyy,[1,4] L.I. Ieremenko,[1] I.V. Tkachenko,[1] K.E. Grinkevich,[1] S.E. Ivanchenko,[1] A.V. Zelinskiy,[2] G.V. Shpakova,[3] and A.V. Ragulya[1]

UDC 621.762.5: 621.762.53

The production of $ZrN–Si_3N_4$ and $ZrN–Si_3N_4–TiN$ composites by spark plasma sintering and the mechanical and tribological properties of the consolidated materials were studied. The densification of the $ZrN–Si_3N_4–TiN$ composites was found to proceed more intensively in the range 1100–1300°C, and nanocrystalline titanium nitride was the main factor that promoted the densification of these composites. Ceramic 57 wt.% ZrN–43 wt.% Si_3N_4 and 84 wt.% ZrN–16 wt.% Si_3N_4 samples with a relative density of 0.95 and 0.93 and (84 wt.% ZrN–16 wt.% Si_3N_4)–15 wt.% TiN and (57 wt.% ZrN–43 wt.% Si_3N_4)–30 wt.% TiN composites with a relative density of ~0.98 were produced. Microstructural studies showed that components of the consolidated $ZrN–Si_3N_4$ composites were uniformly distributed over the material with an average grain size of 200–300 nm. The $ZrN–Si_3N_4–TiN$ composites had a finer structure, TiN grains being smaller than 100 nm. The mechanical properties of the titanium nitride composites were higher than those of the $ZrN–Si_3N_4$ materials. Thus, the Vickers hardness and indentation-determined fracture toughness of the composites containing 15 and 30 wt.% TiN were 18.7 ± 1.1 GPa and 5.2 MPa · $m^{1/2}$ and 19.1 ± 1.9 GPa and 5.8 MPa · $m^{1/2}$, respectively. The hardness of the $ZrN–Si_3N_4$ composites was ~17 GPa. The tribological properties of the composites were tested with the VK6 hardmetal and silicon nitride. The wear resistance of the ceramic samples directly depended on the contents of zirconium nitride and counterface, i.e., on their physicochemical interaction. When the ZrN content increased to 84%, the tribological properties of the composites improved substantially through the lubricating capability of zirconium nitride. The (84 wt.% ZrN–16 wt.% Si_3N_4)–15 wt.% TiN composite showed the best tribological properties and can be recommended for use in friction units under dynamic loads.

Keywords: *spark plasma sintering, composites, wear, Si_3N_4, ZrN, TiN.*

INTRODUCTION

The development of new wear-resistant composites with high tribological characteristics is relevant for modern powder metallurgy and is a necessary precondition for improving the service life of machines and mechanisms, promoting appropriate energy efficiency, and protecting the environment against contamination. The

[1]Frantsevich Institute for Problems of Materials Science, National Academy of Sciences of Ukraine, Kyiv, Ukraine. [2]Ivan Franko National University of Lviv, Lviv, Ukraine. [3]Kyiv National University of Construction and Architecture, Kyiv, Ukraine.

[4]To whom correspondence should be addressed; e-mail: zgalatlozynskyy@gmail.com.

Translated from Poroshkova Metallurgiya, Vol. 60, Nos. 9–10 (541), pp. 95–107, 2021. Original article submitted July 6, 2021.

quality of products made of technical ceramics, including silicon nitride ceramics, depends on the quality of the starting materials and consolidation techniques. The main aspect to be addressed in choosing a ceramic production technique is to ensure that the products reach the highest possible density and the scope of required machining is reduced. Several time-proven sintering techniques, whose choice depends on the material composition, geometric configuration, and sizes and operating conditions of the products, are most often used in commercial production of technical ceramic parts.

The choice of materials and an optimal ratio between the service properties and economic feasibility of production are most important in the design of ceramic-based friction units (for example, hybrid or ceramic bearings). Ceramic composites are most suitable for making wear-resistant parts that perform in extreme conditions with limited or zero lubrication. Among the ceramic materials, except for zirconium oxide, silicon nitride offers the most appropriate combination of properties imparting the greatest wear resistance to silicon nitride materials and allowing their applications to be expanded [1–8].

There are several ways to improve the properties of ceramic materials: refine the grains, introduce new components, and modify the surface [1–3, 5–8].

The Si_3N_4–TiN-based composites showed high mechanical and tribological properties [3, 5–8]. The Si_3N_4–ZrN ceramic composites with high zirconium nitride content [9–14], which are being used to produce wear-resistant coatings that perform in extreme conditions, are quite promising as well. However, the production of bulk wear-resistant ZrN–Si_3N_4 ceramics still has not been studied in a comprehensive manner. This is associated with difficulties in the synthesis of composite powders and with the choice of a method for their consolidation to produce a dense homogeneous ceramic material. The modern synthesis and consolidation techniques permit the production of both fine-grained powder mixtures and dense ceramic materials in the ZrN–Si_3N_4 system [15–18]. For example, spark plasma sintering (SPS) allows rapid consolidation of refractory ceramic materials at temperatures that are much lower than those used in hot pressing or conventional sintering in resistance furnaces [3, 7, 18–20].

The development of new wear-resistant composites with nitride ceramics has long been under discussion [4–6, 21]. Note, however, that the cited friction and wear characteristics vary substantially with testing conditions. Thus, in dry lubrication, the friction coefficient of silicon nitride composites can vary from 0.2 to more than 0.8 depending on testing conditions [1–8]. Numerous factors (atmospheric humidity, temperature, speed, load, and microstructural features) influence the wear mechanisms. Besides the structure (grain size and porosity) and constitution of composites, the choice of friction couples and testing conditions has a substantial effect on the tribological properties [1–8, 22–25].

Therefore, the development of wear-resistant ceramic composites that would perform in extreme conditions (high temperatures) with minimum or zero lubrication is relevant.

Our purpose is to produce ZrN–Si_3N_4 and ZrN–Si_3N_4–TiN composites by spark plasma sintering and examine their tribological properties under dynamic and static loads in sliding against silicon nitride and VK6 hardmetal.

EXPERIMENTAL PROCEDURE

The starting materials were the TiN powder produced by Nanostructured and Amorphous Materials (USA) with an average particle size of 20 nm and a mixture of the ZrN–Si_3N_4 powders produced by the Frantsevich Institute for Problems of Materials Science (Ukraine) with an average particle size of ~200 nm [15–17]. According to the manufacturer's certificate, the oxygen and nitrogen contents of the titanium nitride powder were 0.22 and 21.91 wt.%. The oxygen content of the final product (synthesized ZrN–Si_3N_4 powder mixtures) determined by standard chemical analysis procedure was 2.2 and 2.8 wt.% for the composites with 16 and 43 wt.% Si_3N_4.

We also synthesized ZrN–Si_3N_4 powder mixtures with 57 and 84 wt.% ZrN. A composite material with the Si_3N_4 and ZrN phases being distributed uniformly was produced in a single synthesis cycle from the hardmetal precursor at 1000–1200°C [17].

We also prepared (84 wt.% ZrN–16 wt.% Si_3N_4)–15 wt.% TiN and (57 wt.% ZrN–43 wt.% Si_3N_4)–30 wt.% TiN mixtures in a Pulverizette-6 planetary-ball mill with a silicon nitride drum in ethyl alcohol. The

components were mixed at a three-to-one weight ratio of the silicon nitride balls and powder; the rotation speed was 150 rpm and mixing time 4 h. A vacuum oven was used for drying and alcohol evaporation at 70–80°C for 8 h.

An FCT-HPD25 furnace manufactured by FCT Systems GmbH (2400°C maximum temperature, applied pressure to 250 kN, 8000 A maximum current, 10 V maximum voltage, $5 \cdot 10^{-2}$ Pa vacuum or nitrogen atmosphere) was used for spark plasma sintering of the composites. The temperature was measured by a pyrometer on the inner surface of the upper graphite punch.

The linear shrinkage of the composites consolidated by SPS was recorded as movement of the upper punch (the lower punch was fixed) and converted into the shrinkage rate. About 8 g of the composite powder was poured into a graphite die 20 mm in diameter and 50 MPa pressure was applied to promote stable contacts between the ZrN–Si_3N_4–TiN particles and graphite die. Nonlinear SPS conditions with variation in the heating rate and pressure determined in [18, 20, 26] were used. The ZrN–Si_3N_4 composites were consolidated by SPS in the proposed nonlinear conditions in several stages: in the ranges 20–800, 800–1200, and 1200–1750°C with gradual increase in pressure from 5 to 60 MPa and decrease in the heating rate from 100 to 20°C/min at each stage.

The phase composition of the starting powders and materials after SPS was studied by X-ray diffraction employing a DRON 3M diffractometer with copper radiation. No other phases besides the main ones used to prepare the starting mixtures (Si_3N_4, ZrN, TiN) were found [15–17].

After SPS consolidation, the sintered composites were longitudinally cut and polished for mechanical and tribological analyses. The standard Vickers hardness measurement employing an MMT-3 tester (Buehler, Germany) was performed. The impression diagonal was measured after holding for 15 sec under a load of 19.61 N. The microhardness of the test materials was evaluated from 15 imprints and the root-mean-square measurement error was assessed.

The fracture toughness was determined by indentation with a standard IT 5010 hardness tester (*Tochpribor*, Russia) under a load of 49.03 N. The calculation was performed with the Evans method [27].

Microstructural analysis of the consolidated ceramic samples and their surfaces after tribological tests was carried out by scanning electron microscopy using Vega 3 and Mira 3 microscopes (Tescan).

Tribological wear tests were performed employing an automated tribological dynamic test machine (ATDS) (Fig. 1).

The indenter moved reciprocally over the flat samples with local Hertzian contact and a preliminary determined load component of 30 N (quasistationary or static loading). At an effective load of 30 N (maximum wear reproducibility in both load modes) in dynamic mode, the forces of normal load are set as a train of oscillations for the dynamic load component. The dynamic load component has an amplitude of 5 N, pulse length of $5 \cdot 10^{-2}$ sec, and frequency of 25 Hz. The choice of these parameters ensures that the experimental conditions are as unified as possible and accelerates ATDS tests. A sliding speed of 0.0147 m/sec was chosen to record the friction force as accurately as possible. The roughness profile patterns for the surfaces subjected to wear were used to determine the wear (friction path depth), dispersion (correlating with weight wear), and wear variation coefficients for static and dynamic modes. The friction force was self-recorded on tribological patterns.

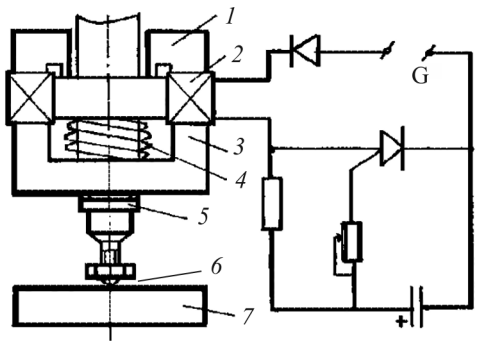

Fig. 1. Schematic diagram of ATDS: *1*) fixed part; *2*) coil; *3*) moving electromagnet part; *4*) spring; *5*) lock ring; *6*) indenter; *7*) sample; G—generator of electric pulses

The tribological properties of the samples were examined in plane–ball tests (dry friction) under indenter static and dynamic loads in accordance with the procedure described in [22–25]. For tribological tests, composite samples were prepared as polished plates approximately 6 mm thick. The counterface (indenter) was balls 8 mm in diameter made of the VK6 hardmetal or Si_3N_4. The testing time was 900 sec and temperature $T = 20$ºC in both cases.

The sample surfaces subjected to tribological tests were studied with a Micron Lambda automatic roughness meter (National Aviation University, Ukraine).

CONSOLIDATION OF THE ZrN–Si_3N_4 AND ZrN–Si_3N_4–TiN COMPOSITE POWDERS

The ZrN–Si_3N_4 and ZrN–Si_3N_4–TiN composite powders were consolidated by SPS in a nitrogen atmosphere to 1750°C. Table 1 summarizes the composition of the starting powders and associated materials.

TABLE 1. Composition of the Starting Powders and Properties of the ZrN–Si_3N_4 and ZrN–Si_3N_4–TiN Composites Consolidated by SPS

Sample No.	Composition of (powder) material, wt.%	Relative density	*HV*2, GPa	Fracture toughness, MPa · $m^{1/2}$
1	57 ZrN–43 Si_3N_4	0.95	17.3 ± 1.5	–
2	84 ZrN–16 Si_3N_4	0.93	16.9 ± 2.2	–
3	(84 ZrN–16 Si_3N_4)–15 TiN	0.97	18.7 ± 1.1	5.2
4	(57 ZrN–43 Si_3N_4)–30 TiN	0.98	19.1 ± 1.9	5.8

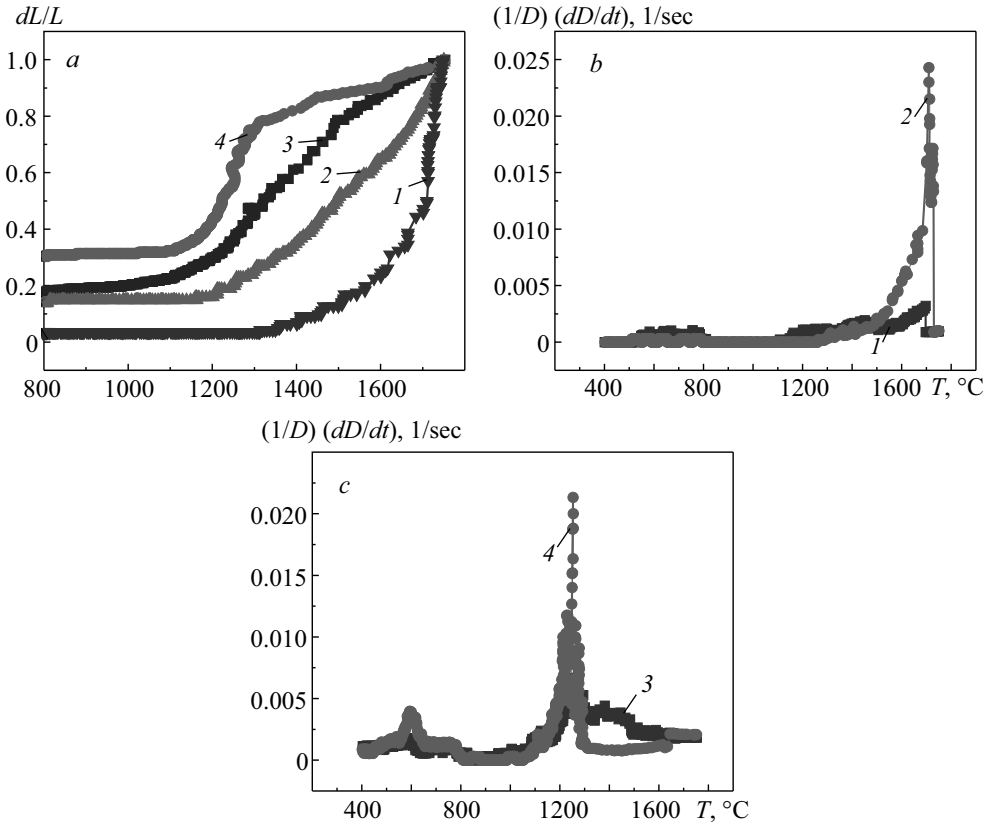

Fig. 2. Densification *dL*/*L* (*a*) and densification rate versus sintering temperature of the ZrN–Si_3N_4 (*b*) and ZrN–Si_3N_4–TiN (*c*) composite powders in SPS: curve numbers correspond to sample numbers in Table 1

The temperature dependence of shrinkage is shown in Fig. 2*a*. The ZrN–Si_3N_4 composite powders (Fig. 2*a*, curves *1* and *2*) were consolidated first. The 57 ZrN–43 Si_3N_4 composite, characterized by an almost equal ratio of components, starts consolidating at ~1300ºC (Fig. 2*a*, curve *1*), and the maximum densification rate is reached at 1700ºC (Fig. 2*b*, curve *1*). At the same time, densification of the composite with lower silicon nitride content, 84 ZrN–16 Si_3N_4, begins at ~1180ºC (Fig. 2*a*, curve *2*) and proceeds with almost the same speed to 1700ºC (Fig. 2*b*, curve *2*). The higher densification rate of the 84 ZrN–16 Si_3N_4 material is due to a greater content of the phase with high electrical conductivity (ZrN). Similar results were reported in [15, 16], focusing on the synthesis and SPS of the ZrN–Si_3N_4 composite powders with 33, 22, and 11 vol.% ZrN up to 1750ºC. For complete densification of the test materials, greater temperatures (~1800ºC) or isothermal holding at high temperatures are needed.

To intensify the densification of the composites, 15 and 30 wt.% of the nanocrystalline titanium nitride powder were added to the starting ZrN–Si_3N_4 powder mixtures. The densification of the ZrN–Si_3N_4–TiN composites starts at ~1000ºC (Fig. 2*a*, curves *3* and *4*) and proceeds at ~0.015–0.023 1/sec in the range 1100–1300ºC (Fig. 2*c*). Nanocrystalline titanium nitride is the main factor that promotes the densification process in this temperature range [8, 18, 20]. The maximum densification rate, ~0.0025 1/sec (Fig. 2*c*, curve *3*), is observed for the (84 ZrN–16 Si_3N_4)–15 TiN composite at ~1400ºC, which is similar to the densification of the ZrN–Si_3N_4 composite powders (Fig. 2*b*). This maximum is characteristic of zirconium nitride densification by SPS [28].

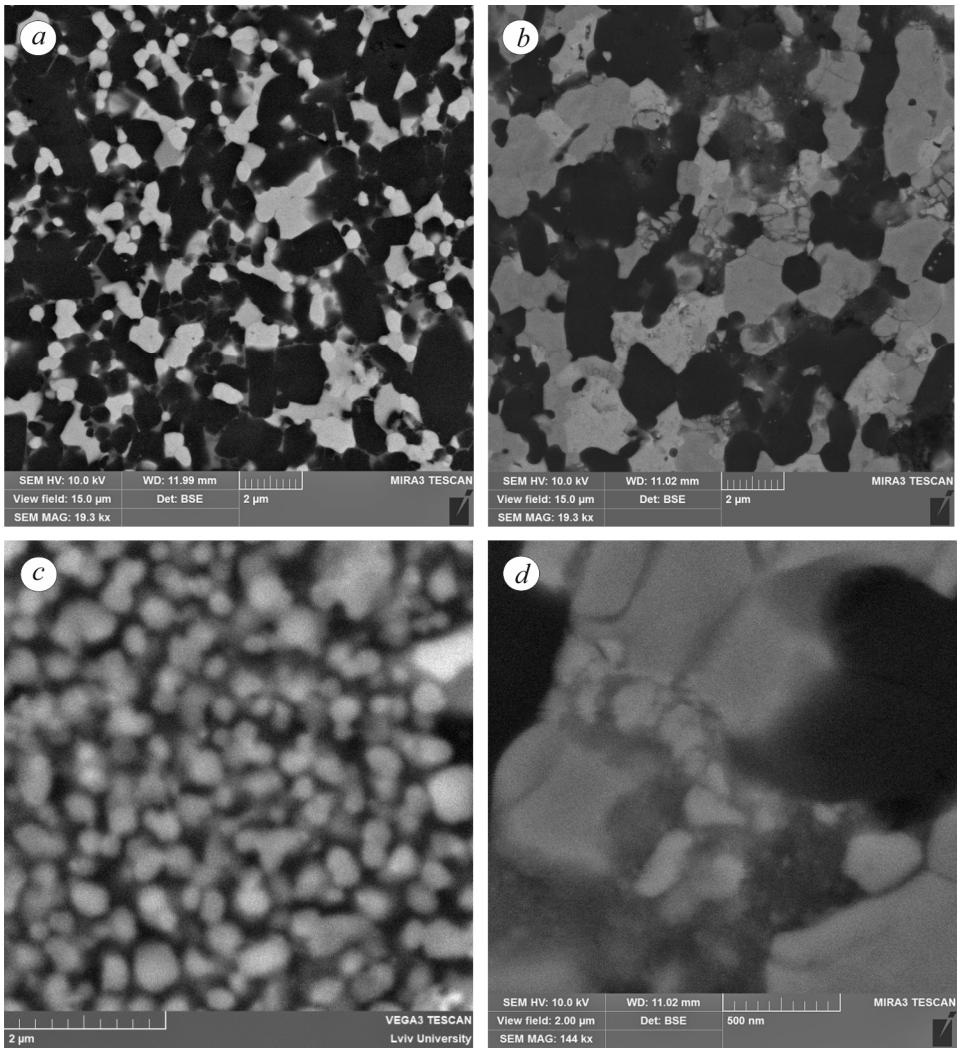

Fig. 3. Microstructure of the composites, wt.%: *a*) 57 ZrN–43 Si_3N_4; *b*, *d*) (57 ZrN–43 Si_3N_4)–30 TiN; *c*) (84 ZrN–16 Si_3N_4)–15 TiN

The mechanical properties of the composites (Table 1) depend on their microstructure and residual porosity. Thus, considering high residual porosity, hardness of the ZrN–Si_3N_4 composites is 16–17 GPa (Table 1). At the same time, composites with titanium nitride showed an increase in hardness to 19 GPa and their fracture toughness was 5.2 and 5.8 MPa · $m^{1/2}$ at 15 and 30 wt.% TiN, accordingly (Table 1). Information only on the mechanical properties of the Si_3N_4–TiN, Sialon–ZrN, and ZrN composites consolidated by SPS was published previously [3, 5–10]. Studies of tribological properties focused only on films in the Si–Zr–N system [11–14].

In studying the SPS consolidation of the ZrN powders in different process conditions (T_{sint} = 1400–1700ºC, P = 30–120 MPa), it was shown in [28] that the grain size and porosity influenced the mechanical properties of

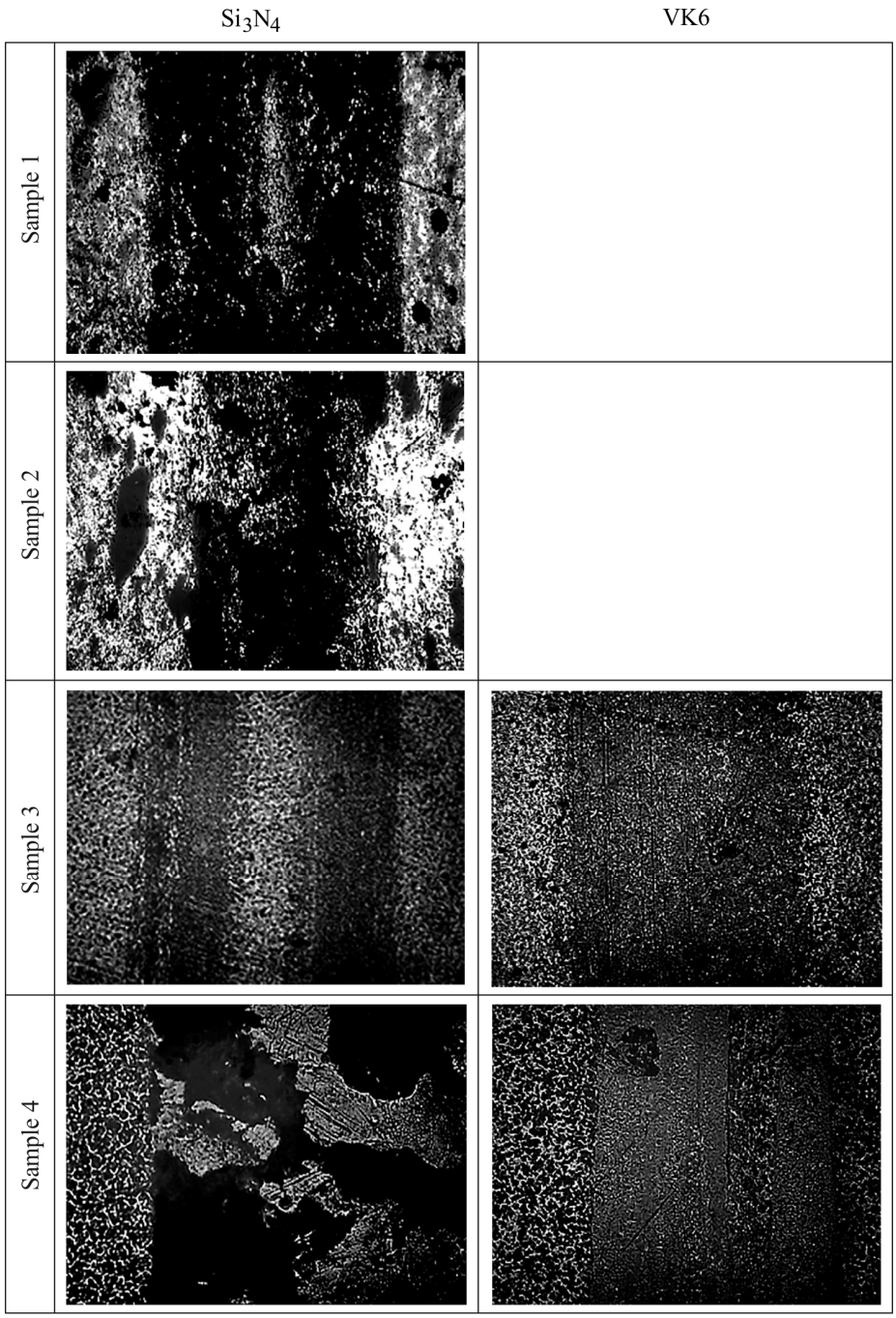

Fig. 4. Characteristic sections of the friction paths of samples 3–4 (Table 1) with the Si_3N_4 and VK6 counterface; ×56

zirconium nitride. The highest hardness, *HV*1 ~ 15 GPa, was shown by the sample with an average grain size of ~33 μm that was consolidated by SPS to 1700ºC at P = 60 MPa [28]. Increase in the hardness of the ZrN–Si_3N_4 composites to ~17 GPa (Table 1) was due to finer structure (Fig. 3*a*, *b*).

The mechanical properties of the ZrN–Si_3N_4–TiN composites (Table 1) are commensurable with those of the fine Si_3N_4–TiN and Sialon–ZrN composites [3, 5–9, 19, 28]. Thus, the paper [20] shows that hardness of the Si_3N_4–TiN composites improves to 20–24 GPa with finer grains and with increase in the titanium nitride content to 40 wt.%.

Microstructural analyses indicated that the 57 wt.% ZrN–43 wt.% Si_3N_4 composite was characterized by uniform distribution of components over the volume (Fig. 3*a*); the average grain size was 200–300 nm. The ZrN–Si_3N_4–TiN composites are also characterized by uniform distribution of the components, when finer titanium nitride grains ~100 nm in size are observed against the background of submicron Si_3N_4 and ZrN grains (Fig. 3*d*). Hence, addition of nanocrystalline titanium nitride to the ZrN–Si_3N_4 composite not also substantially promotes the densification of the materials (Fig. 2*c*) but also leads to a finer structure (Fig. 3*d*) and improves the mechanical properties (Table 1).

TRIBOLOGICAL PROPERTIES OF THE ZRN–SI_3N_4 AND ZRN–SI_3N_4–TIN COMPOSITES

Characteristic sections of the friction paths resulting from tribological tests are shown in Fig. 4. Effect of the counterface material (Si_3N_4 and VK6) on contribution of the adhesion interaction between the sample and counterface was examined for samples 3 and 4 (Fig. 4), considering their high mechanical properties (Table 1). The friction path depth was determined by surface profile recording and the path geometry and roughness by 3D surface

TABLE 2. Tribological Properties of the ZrN–Si_3N_4 and ZrN–Si_3N_4–TiN Composites Consolidated by SPS

Sample No.	Si_3N_4 counterface		VK6 counterface	
	Friction coefficient	Wear, μm	Friction coefficient	Wear, μm
1	0.85 / 0.19*	0.85 / 0.85	–	–
2	0.89 / 0.18	0.7 / 0.6	–	–
3	0.56 / 0.11	0.3 / 0.12	0.4 / 0.08	0.16 / 0.08
4	1.62 / 0.18	2.4 / 1.75	0.5 / 0.11	0.3 / 0.2

*Values for testing under static loading/dynamic loading.

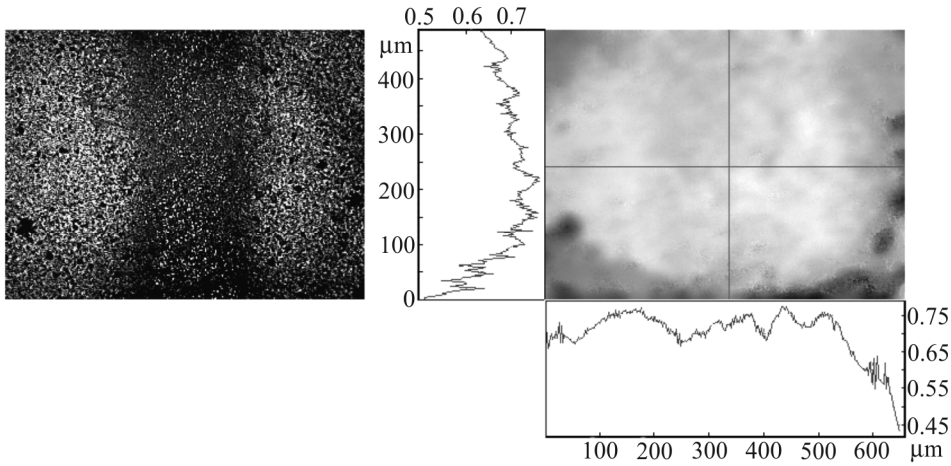

Fig. 5. Surface analysis of sample 3 after friction against the VK6 counterface

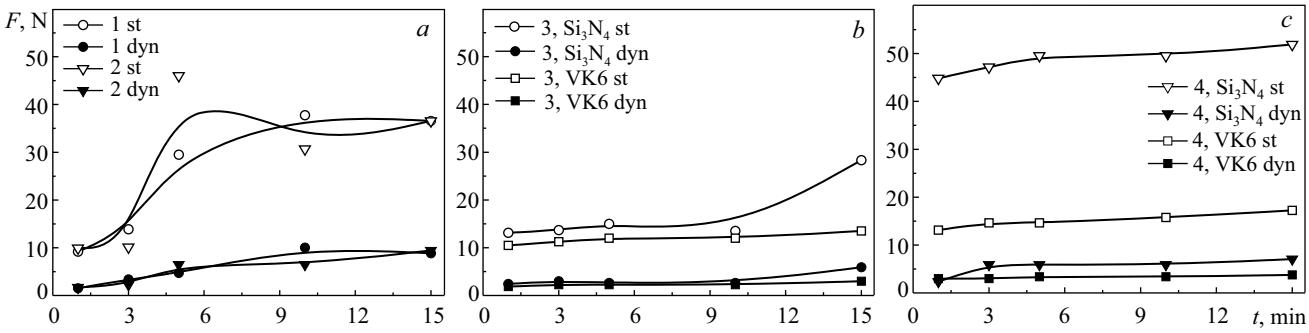

Fig. 6. Friction force of samples 1 and 2 in testing with the Si_3N_4 counterface (*a*) and samples 3 (*b*) and 4 (*c*) with the Si_3N_4 and VK6 counterface under static (st) and dynamic (dyn) indenter load

profile measurement (Fig. 5). The results of tribological tests for the ceramic samples are shown in Figs. 6–8 and Table 2.

Note that adhesive wear in interaction with the Si_3N_4 counterface is predominant in the ZrN–Si_3N_4 system (Fig. 4, samples 1 and 2), which is confirmed by a significant friction force (Fig. 6). Similar reliefs of the friction paths and a significant number of seizure sections were observed in the friction area of the ZrN–Si_3N_4 composites (Fig. 4, samples 1 and 2).

Figure 7 indicates that sample 2 containing 84% zirconium nitride, promoting significant lubrication in the tribological system, has higher wear resistance than sample 1 containing 57% zirconium nitride. However, addition of 15 wt.% TiN to the composite exerted a positive effect on its wear resistance; this is confirmed by 2.5 times lower wear in quasistatic testing conditions and 4 times lower wear in dynamic conditions.

Analysis of the tribological systems containing composites with titanium nitride revealed that addition of 15 wt.% nanocrystalline TiN to ZrN–Si_3N_4 positively influenced its wear resistance and surface relief (Fig. 4, sample 3). This is due to increase in the relative density of the material resulting from addition of titanium nitride (Table 1) and a sufficient amount of zirconium nitride that ensures the lubricating effect in the tribological system. At the same time, when titanium nitride content increases in the ceramics to 30% (sample 4), the wear resistance decreases. This is associated with decrease in the zirconium nitride in the composite, and increase in the Si_3N_4 content leads to interaction with the counterface material (Si_3N_4) and seizure and brittle fracture effects (Fig. 4,

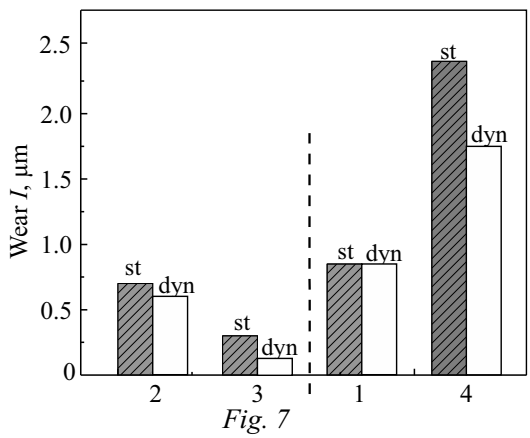

Fig. 7

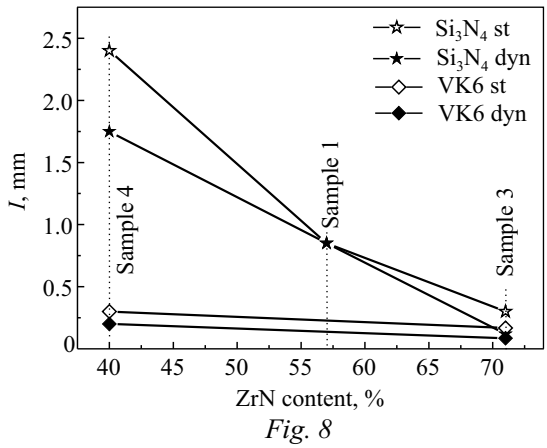

Fig. 8

Fig. 7. Effect from the content of TiN addition on the wear resistance of ceramic samples 1–4 in the ZrN–Si_3N_4 system under static (st) and dynamic (dyn) loading with the Si_3N_4 counterface

Fig. 8. Wear of ceramic samples 1, 3, and 4 depending on the ZrN content under static (st) and dynamic (dyn) loading with the Si_3N_4 and VK6 counterfaces

sample 4). As a result, the friction force increases for the (57 ZrN–43 Si_3N_4)–30 TiN composite, especially in quasistatic testing conditions (Fig. 6).

Note that the physicochemical interaction between the sample and counterface has proved to be decisive for tribological indicators of samples 3 and 4 in friction against the VK6 hardmetal (Fig. 8). The higher the Si_3N_4 content in the ceramic sample, the greater the contribution of the adhesion interaction between the sample and ceramic counterface to the friction force and wear (Figs. 6–8).

As is the case with the Si_3N_4 counterface, the wear resistance of the composite in friction against the VK6 hardmetal significantly increases with higher content of zirconium nitride (Fig. 8); zirconium nitride ensures substantial lubricating capacity in the tribological system, which is confirmed by behavior of the friction force (Fig. 6*b*, *c*). Consider also that quite fine wear products, commensurable with the composite grain sizes, formed during tribological tests. Analyzing this effect, the authors [5] note that fine particles—wear products of the tribological pair—cover the counterface in the 'nanoceramic Si_3N_4–TiN–VK6 counterface' tribological system to form the ceramic–ceramic tribological pair, significantly decreasing its friction coefficient and total wear. We observed a similar effect in the ZrN–Si_3N_4 composites and the composite with 15 wt.% TiN (Fig. 5). Contrastingly, for the composites with high titanium nitride content, there may be rather intensive wear of the friction pair, resulting from predominant content of hard abrasive particles of titanium nitride in the wear products [29].

Therefore, the 'ceramic–VK6' tribological system proved to be more adaptable for use, having, in particular, lower wear and friction coefficient, while the Si_3N_4 amount in the material turned out to be crucial for the 'ceramic–Si_3N_4' tribological system.

CONCLUSIONS

The ZrN–Si_3N_4 and ZrN–Si_3N_4–TiN powder composites have been consolidated by spark plasma sintering to 1750ºC. The 84 ZrN–16 Si_3N_4 composite begins to densify at ~1180ºC in the SPS process almost at the same rate to 1700ºC. The 57 ZrN–43 Si_3N_4 composite shows higher densification rate. The ZrN–Si_3N_4–TiN composites densify more intensively in the range 1100–1300ºC. Nanocrystalline titanium nitride is the main factor that promotes their densification.

Microstructural analysis indicates that components with an average grain size of 200–300 nm are uniformly distributed throughout the 57 ZrN–43 Si_3N_4 composite. Fine titanium nitride grains (~100 nm) are observed in the ZrN–Si_3N_4–TiN composites against the background of submicron Si_3N_4 and ZrN grains (~300 nm). High mechanical properties (~19 GPa *HV*2, ~5.8 MPa · $m^{1/2}$ fracture toughness) are reached when titanium nitride is added to the composites.

When zirconium nitride content in the composites increases to 84%, their tribological properties improve significantly through the lubricating capability of zirconium nitride. At the same time, greater Si_3N_4 content leads to intensive interaction with the counterface material, resulting in seizure effect and, as a result, substantial increase in the friction force. High titanium nitride content in the composite can cause abrasive wear of the friction pair. The (84 ZrN–16 Si_3N_4)–15 TiN composite is the most optimal for performance in dry friction conditions.

ACKNOWLEDGMENTS

The authors are grateful to I.V. Kud, L.A. Krushynska, and D.P. Zyatkevych (Frantsevich Institute for Problems of Materials Science, Ukraine) for provision of the ZrN–Si_3N_4 powder and to Materials Lab LLC for assistance in examining the samples.

REFERENCES

1. D. Kandaswamy, A.C. Krithika, and E.S. Sathish, "Wear analysis of nano ceramic composites against a ceramic antagonist," *J. Conserv. Dent*., **9**, No. 4, 152–158 (2006).
2. J. Olofsson, T.M. Grehk, and T. Berlind, "Evaluation of silicon nitride as a wear resistant and resorbable alternative for total hip joint replacement," *Biomatter*, No. 2, 94–102 (2012).

3. Ingrid Schulz, Mathias Herrmann, Ingolf Endler, Ilmars Zalite, Bruno Speisser, and Johannes Kreusser, "Nano Si_3N_4 composites with improved tribological properties," *Lubr. Sci.*, **21**, 69–81 (2009).
4. B. Zhao, I. Khader, R. Raga, U. Degenhardt, and A. Kailera, "Tribological behavior of three silicon nitride ceramics in dry sliding contact against Inconel 718 over a wide range of velocities," *Wear*, **448–449**, 203−206 (2020).
5. O.B. Zgalat-Lozynskyy, N.I. Tischenko, V.T. Varchenko, A.V. Ragulya, and A.V. Polotai, "Tribological behavior of Si_3N_4-based nanocomposites," *Tribol. Int.*, No. 91, 85−93 (2015).
6. L. Chien-Cheng and H. Jow-Lay, "Influence of TiN particles on the wear behavior of silicon nitride–based composites," *J. Mater. Res.*, **19**, No. 2, 542–549 (2004).
7. V.G. Kolesnichenko, O.B. Zgalat-Lozinskii, V.T. Varchenko, M. Herrmann, and A.V. Ragulya, "Friction and wear of TiN–Si_3N_4 nanocomposites against ShKh15 steel," *Powder Metall. Met. Ceram.*, **53**, No. 11−12, 680–687 (2015).
8. O.B. Zgalat-Lozynskyy, K.S. Apurbba, I.I. Egorov, V.T. Varchenko, and K.S. Suresh, "Wear-resistant TiN–20 wt.% Si_3N_4 and TiN–20 wt.% TiB_2 composites produced by microwave sintering," *Powder Metall. Met. Ceram.*, **59**, No. 11–12, 611–620 (2021).
9. L. Yin and M.I. Jones, "Fabrication and properties of Sialon-ZrN composites by two-step sintering," *Int. J. Refract. Met. Hard Mater.*, **92**, 1–8 (2020).
10. R.W. Harrison and W.E. Lee, "Processing and properties of ZrC, ZrN and ZrCN ceramics: a review," *Adv. Appl. Ceram.*, **115**, No. 5, 294–307 (2016).
11. R. Vishnu, J. Das, S.B. Arya, and R. Manish, "Electrochemical corrosion behavior of ZrN film in various corrosive fluid," *Int. J. Surf. Eng. Interdiscip. Mater. Sci.*, **3**, No. 1, 1−13 (2015).
12. Z. Wu, X. Zhong, C. Liu, Z. Wang, W. Dai, and Q. Wang, "Plastic deformation induced by nano-indentation test applied on ZrN/Si_3N_4 multilayer coatings," *Coatings*, **8**, 1–11 (2018).
13. L. Rogström, L.J.S. Johnson, M.P. Johansson, M. Ahlgren, L. Hultman, and M. Odén, "Thermal stability and mechanical properties of arc evaporated ZrN/ZrAlN multilayers," *Thin Solid Films*, **519**, 694–699 (2010).
14. M.S. Wong, G.Y. Hsiao, and S.Y. Yang, "Preparation and characterization of AlN/ZrN and AlN/TiN nanolaminate coatings," *Surf. Coat. Technol.*, **133–134**, 160–165 (2000).
15. I. Kud, L. Ieremenko, L. Krushynska, D. Zyatkevych, O. Zgalat-Lozynskyi, and O. Shyrokov, "Synthesis and consolidation of powders based on Si_3N_4–Zr. Nanooptics and photonics, nanochemistry and nanobiotechnology, and their applications," *Springer Proc. Phys.*, **247**, 23–33 (2020).
16. I.V. Kud, L.I. Eremenko, L.A. Krushynska, O.V. Shirokov, O.B. Zgalat-Lozynskyy, D.P. Zyatckevych, and I.V. Uvarova, "Composite powders in the Si_3N_4–ZrN system for electrical applications," *Elektr. Kont. Elektrod.*, No. 14, 31–38 (2018).
17. I.V. Kud, L.I. Eremenko, L.A. Krushynska, D.P. Zyatkevych, O.B. Zgalat-Lozynskyy, O.V. Shyrokov, and L.S. Protsenko, "Synthesis of groundless Si_3N_4–ZrN composite powder," *Dop. Nats. Akad. Nauk Ukrainy*, No. 1, 54–60 (2020).
18. O.B. Zgalat-Lozynskyy, A.V. Ragulya, M. Herrmann, M. Andrzejczuk, and A. Polotai, "Structure and mechanical properties of spark plasma sintered TiN-based nanocomposites," *Arch. Metall. Mater.*, **57**, No. 3, 853–858 (2012).
19. O. Zgalat-Lozynskyy, M. Andrzejczuk, V. Varchenko, M. Herrmann, A. Ragulya, and A. Polotai, "Superplastic deformation of Si_3N_4 based nanocomposites reinforced by nanowhiskers," *Mater. Sci. Eng.*, **606**, 144–149 (2014).
20. O.B. Zgalat-Lozinksii, "Nanocomposites based on refractory compounds, consolidated by rate-controlled and spark-plasma sintering (Review)," *Powder Metall. Met. Ceram.*, **53**, No. 1–2, 19-30 (2014).
21. J. Vizintin, M. Kalin, S. Novak, G. Draii, L.K. Ives, and M.B. Peterson, "Effect of slip amplitude on the fretting wear of silicon nitride against silicon nitride," *Wear*, **192**, 11–20 (1996).

22. R.K. Nevshupa, K.E. Grinkevych, and R.I. Martinez, “TriDes—a new tool for the design, development and non-destructive evaluation of advanced construction steels,” *Mater. Constr*., **66**, No. 324, e099 (2016).
23. D.A. Lesyk, S. Martinez, B.N. Mordyuk, V.V. Dzhemelinskyi, A. Lamikiz, G.I. Prokopenko, K.E. Grinkevych, and I.V. Tkachenko, “Laser-hardened and ultrasonically peened surface layers on tool steel AISI D2: correlation of the bearing curves’ parameters, hardness and wear,” *J. Mater. Eng. Perform.*, **27**, No. 2, 764–776 (2018).
24. K. Nakano, K. Kawaguchi, K. Takeshima, Y. Shiraishi, F. Forsbach, J. Benad, M. Popovand, and V.L. Popov, “Investigation on dynamic response of rubber in frictional contact,” *Front. Mech. Eng*., **5**, 1–9 (2019).
25. K. Grinkevich, “Some postulates of the structural dynamic concept of the tribo-system and its practical implementation,” *Frict. Wear*, **24**, No. 3, 100–106 (2003).
26. O. Zgalat-Lozynskyy, M. Herrmann, and A. Ragulya, “Spark plasma sintering of TiCN nanopowders in non-linear heating and loading regimes,” *J. Eur. Ceram. Soc*., **31**, 809–813 (2011).
27. H. Miyazaki, Y.-I. Yoshizawa, and K. Yasuda, “Improved accuracy of the measurements of indentation fracture resistance for silicon nitride ceramics by the powerful optical microscopy,” *Ceram. Int.*, **39**, 9499–9504 (2013).
28. G. Lee, M.S. Yurlova, D. Giuntini, E.G. Grigoryev, O.L. Khasanov, J. McKittrick, and E.A. Olevsky, “Densification of zirconium nitride by spark plasma sintering and high voltage electric discharge consolidation: a comparative analysis,” *Ceram. Int*., **41**, 14973–14987 (2015).
29. J. Tatami, E. Kodama, H. Watanabe, H. Nakano, T. Wakihara, et al., “Fabrication and wear properties of TiN nanoparticle-dispersed Si_3N_4 ceramics,” *J. Ceram. Soc. Japan*., **116**, 749–54 (2008).